CFD Simulation of Valve Closing

Best Practice Guide

Tomáš Blejchař

Ostrava, 2022

VSB TECHNICAL UNIVERSITY OF OSTRAVA
IT4INNOVATIONS NATIONAL SUPERCOMPUTING CENTER

Table of contents

Nomenclature

c_v	Specified heat at constant volume	$[J/(m^3 \cdot K)]$
c_p	Specified heat at constant pressure	$[J/(kg \cdot K)]$
$c_{1\varepsilon}$	Empirical constant	$[1]$
$c_{2\varepsilon}$	Empirical constant	$[1]$
$c_{3\varepsilon}$	Empirical constant	$[1]$
C_2	Constant	$[1]$
C_D	Empirical constant	$[1]$
C_υ	Constant	$[1]$
C_μ	Constant	$[1]$
C_η	Empirical constant	$[1]$
D_i	Diffusion coefficient	$[m^2/s]$
E	Energy	$[J/kg]$
G	Thermic production of turbulent kinetic energy	$[m^2/s^3]$
G_b	Production of turbulent kinetic energy due buoyancy	$[kg/(m \cdot s^3)]$
G_k	Production of turbulent kinetic energy due velocity gradient	$[kg/(m \cdot s^3)]$
G_υ	Production of turbulnt viscosity	$[kg/(m \cdot s^2)]$
g	Gravity acceleration	$[m/s^2]$
h	Enthalpy	$[J/kg]$
h	Cell height	$[m]$
I	Spectral radiation intensity	$[W/(sr \cdot m)]$

k	Turbulent kinetic energy	$[\mathrm{m}^2/\mathrm{s}^2]$
K	Reaction rate constant	$\left[(\mathrm{mol}\cdot\mathrm{m}^{-3})^{1-\mathrm{n}}\cdot\mathrm{K}^{\beta}/s\right]$
M	Molar mass	$[\mathrm{kg/kmol}]$
Ma	Mach number	$[1]$
m	mass	$[\mathrm{kg}]$
n	Substance amount	$[\mathrm{kmol}]$
n	Reaction order	$[1]$
P	Mechanical production of turbulent kinetic energy	$[\mathrm{m}^2/\mathrm{s}^3]$
p	Pressure	$[\mathrm{Pa}]$
p_a	Atmospheric pressure	$[\mathrm{Pa}]$
Pr_t	Prandtl turbulent number	$[1]$
Q	Volume flow	$[\mathrm{m}^3/\mathrm{s}]$
Q_m	Mass flow	$[\mathrm{kg/s}]$
r	Radius vector	$[\mathrm{m}]$
Re	Reynolds number	$[1]$
R	Universal gas constant	$[\mathrm{J}/(\mathrm{K}\cdot\mathrm{kmol})]$
R_i	Production rate of i^{th} species due chemical reaction	$[\mathrm{kg}/(\mathrm{m}^3\cdot\mathrm{s})]$
r	Gas constant	$[\mathrm{J}/(\mathrm{kg}\cdot\mathrm{K})]$
S	Surface, Area	$[\mathrm{m}^2]$
$\mathrm{S_i}$	Production rate of distributed species	$[\mathrm{kg}/(\mathrm{m}^3\cdot\mathrm{s})]$
$\mathrm{Sc_t}$	Schmidt turbulent number	$[1]$

S_k	Users defined source term of turbulent kinetic energy	$[\mathrm{kg/(m{\cdot}s^3)}]$
S_ε	Users defined source term of dissipation rate	$[\mathrm{kg/(m{\cdot}s^4)}]$
S_υ	Users defined source term of viscosity	$[\mathrm{kg/(m{\cdot}s^2)}]$
T	Thermodynamic temperature	$[\mathrm{K}]$
T^*	Dimensionless temperature	$[1]$
t	Relative temperature	$[°\mathrm{C}]$
t	Time	$[\mathrm{s}]$
u	velocity	$[\mathrm{m/s}]$
u_i	i^{th} component of velocity	$[\mathrm{m/s}]$
$\overline{u_i}$	i^{th} component of mean velocity	$[\mathrm{m/s}]$
x_i	Coordinates $[x_1, x_2, x_3]$ nebo [x, y, z]	$[\mathrm{m}]$
X_i	Molar fraction of i^{th} component of mixture	$[1]$
Y_i	Mass fraction of i^{th} component of mixture	$[1]$
Y_M	Fluctuation dilatation source term	$[\mathrm{kg/(m{\cdot}s^3)}]$

Greek letters:

δ_{i3}	Kronecker delta	$[1]$
ε	Dissipation rate	$[\mathrm{m^2/s^3}]$
γ	Heat capacity ratio, Adiabatic index	$[1]$
λ	Thermal conductivity	$[\mathrm{W/(m \cdot K)}]$
η	Dynamic viscosity	$[\mathrm{Pa \cdot s}]$
η_{eff}	Effective viscosity	$[\mathrm{Pa \cdot s}]$
η_t	Turbulent viscosity	$[\mathrm{Pa \cdot s}]$

υ	Viscosity	$[m^2/s]$
υ_t	Turbulent viscosity	$[m^2/s]$
ρ	Density	$[kg/m^3]$
τ	Shear stress	[Pa]
τ_{jl}	Shear stress tensor	[Pa]
σ_k	Empirical constant	[1]
σ_ε	Empirical constant	[1]

List of Abbreviations:

CFD	Computation Fluid Dynamics
LES	Large Eddy Simulation
RANS	Reynolds Average Navier-Stokes
RNG	Re-Normalization Group

1 Introduction

The interaction of fluid and solid bodies has been studied since the antics ages. Greek Philosophers like Aristoteles or Archimedes studied fluid flow and the interaction of the fluid with immersed bodies. Interaction of fluid and solid bodies occurs in many physical branches like power engineering, automotive, hydromechanics, aerodynamics etc. Nowadays, numerical methods like the Finite Volume Method (FVM), Finite Element Method (FEM), Smoothed-particle hydrodynamics (SPH), etc. are used to perform simulations of fluid flow. The main result of these simulations is a prediction of forces acting on the solid body. The main result of these simulations is a prediction of forces and torques acting on the solid body. Estimated forces and torques are often used to design actuators or structures supporting solid bodies.

This report deals with the simulation of flow in a shut-off valve and torque acting on the flap of the valve, respectively. The first step involved studying all possibilities of fluid-solid interaction simulation using the Computational Fluid Dynamics (CFD) approach. A simplified flap was designed to perform Fluid-Structure Interaction (FSI) and moving mesh method testing. The flap geometry did not involve geometry entities which would limit any method of FSI. The dimensionless numbers were applied to the problem and a simple description of physics.

2 Moving solid body problem

Moving body and solid boundary, respectively, can be generally simulated by two different approaches:

1) mesh modification i.e., moving, and deforming mesh

2) overset meshes i.e., overset mesh and immersed body.

They can be used to study stationary states and time-dependent deformations where the geometry changes its shape due to the motion of solid boundaries and the deformation of solid domains.

2.1 Moving mesh method

The moving mesh method splits the domain into stationary and moving frames. The domains are connected via an interface, and the moving frame slides along the stationary frame (see figure 2.1 for reference). The fluid flow is solved separately in stationary and moving frames, and both simulations are coupled via the nonconformal interface. This method is useful for the simulation of cases with simple rectilinear or rotary motion, e.g., pump impeller rotation, opening or closing of a ball valve, opening or closing of a spool valve, rotor-stator passing in turbomachinery etc.

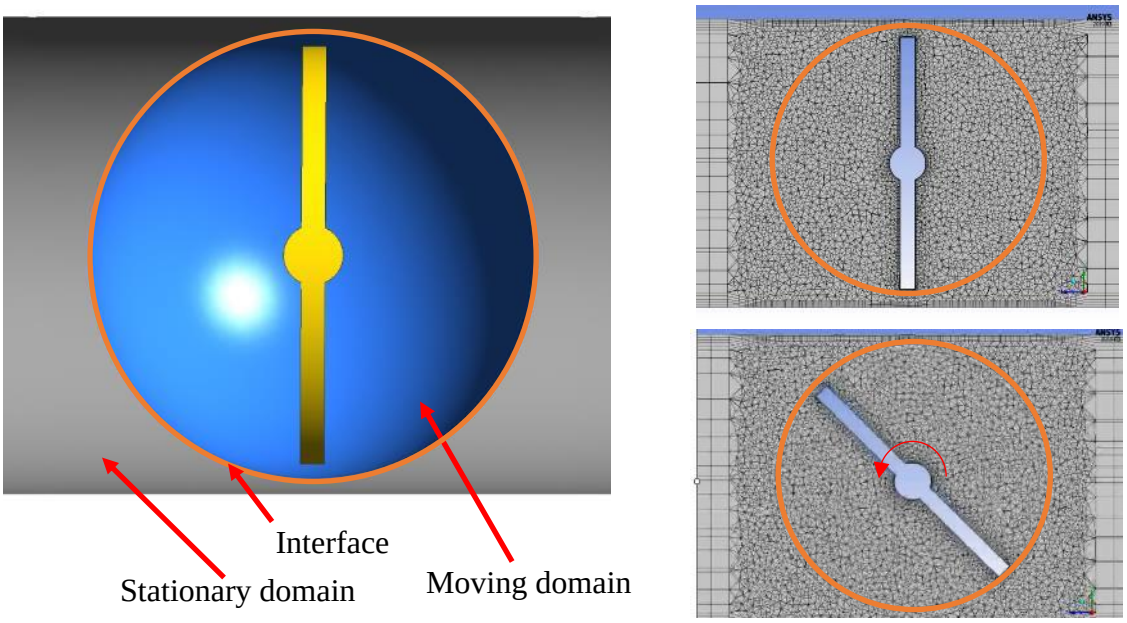

Fig. 2.1 Moving mesh

2.2 Dynamic mesh method

The dynamic mesh model can simulate flows where the shape of the domain changes with time due to motion on the solid body and its domain boundaries, respectively. Combined with the six degrees of freedom (6 DOF) solver, dynamic mesh allows the simulation of the trajectory of a moving object caused by the hydrodynamic forces from the surrounding flow field. The elementary capabilities are three dynamic mesh schemes: smoothing, layering, and remeshing. Combining these three schemes is used to solve the most challenging dynamic mesh problems. The mesh Smoothing and Remeshing method provide instant mesh deformation capability. The dynamic mesh technique consists of three steps:

1. determining dynamic mesh methods,
2. specifying specific modes with dynamic mesh options,
3. defining the dynamic mesh zone.

So, it means mesh is split into the stationary zone and the zone with deformed mesh. Both domains are connected. Thus, no interface is necessary, and interpolation of solution between two domains is performed. The contact of boundaries is not allowed, which creates a restriction in some cases, e.g., simulation with a fully closed valve is impossible.

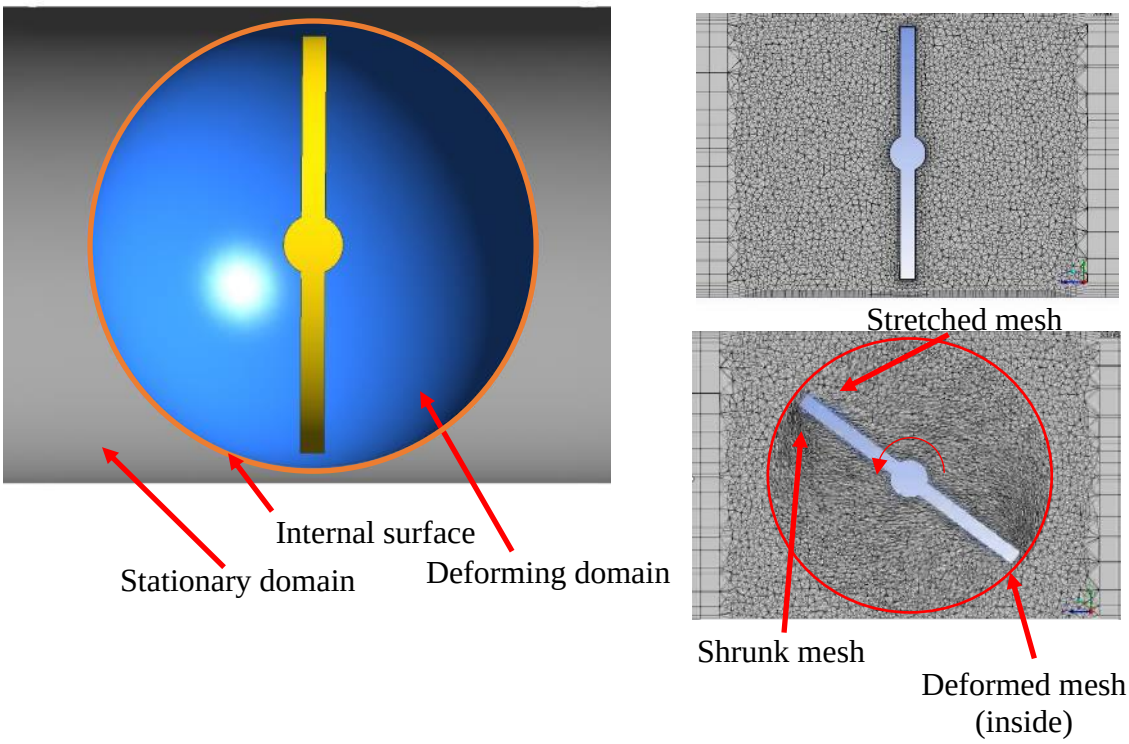

Fig. 2.2 Deforming mesh

2.3 Overset mesh method

Overset mesh, also known as "chimaera" or "overlapping" mesh, is a method based on the solution of the flow field on two independent meshes which overlap each other. Overset mesh can be handy in cases when a large relative motion between components occurs. Compared to remeshing, overset mesh allows greater control of local mesh characteristics as the geometry moves through the domain. Individual mesh zones need not deform to accommodate moving geometry. When used appropriately, the overset mesh can optimise local cell types and quality, reduce cell count (and, therefore, computation time), or simplify model setup. The simulation with overset mesh includes two independent meshes (no interface, no connection). The first is background mesh, containing boundary conditions like inlet, outlet, stationary walls, etc. This mesh represents a free stream without moving the body, and it can be relatively coarse. The second mesh is called foreground mesh and contains boundary conditions (walls) representing the moving body. This mesh is usually fine to precisely describe the shape of the body. This mesh does not usually contain inlet or outlet boundary conditions.

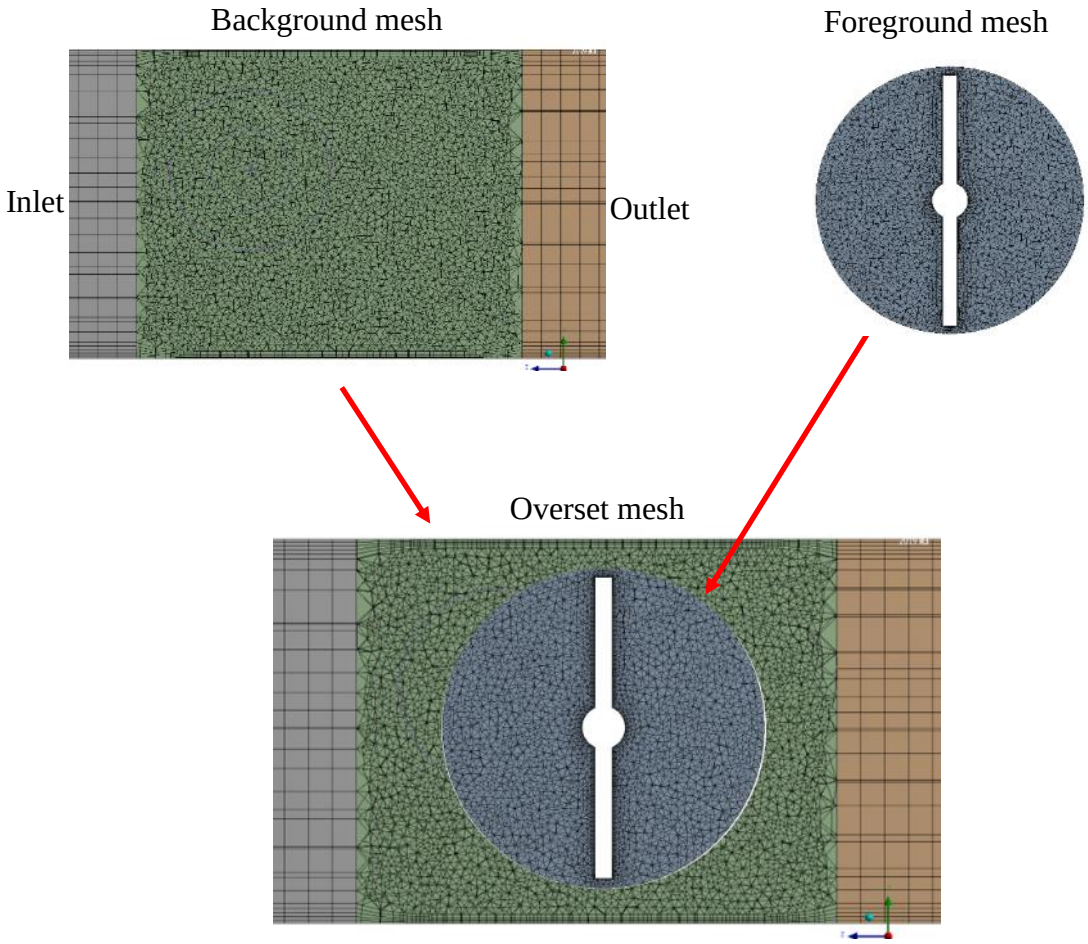

Fig. 2.3 Overset mesh

2.4 Immersed body method

Immersed body method is very similar to overset mesh. The difference is that immersed body method contains solid body mesh instead of fluid mesh surrounding a solid body's outline. The solid mesh can pass through the fluid mesh without limitation. So, this method is easy to use and very robust. If the solid and fluid mesh overlaps, the fluid's main physical properties are set to zero, e.g., velocity. The disadvantage is the necessity of a fine fluid

mesh to respect the outline of a solid body overlapped with fluid.

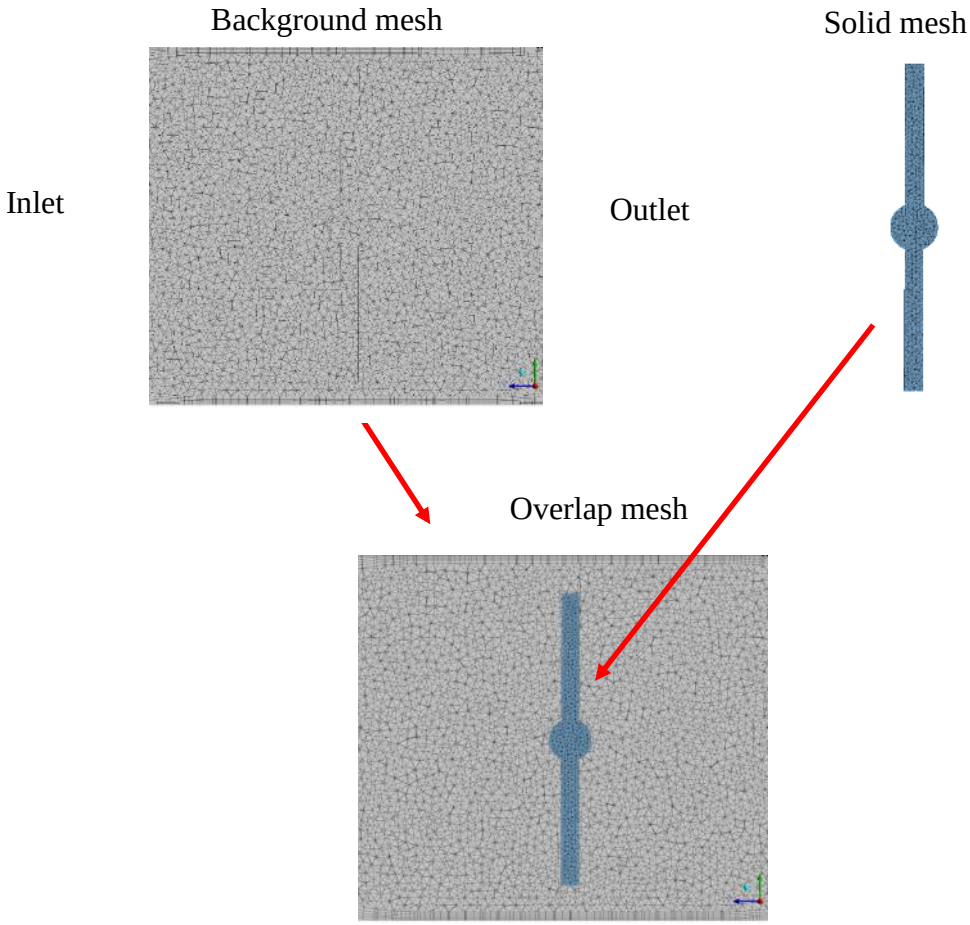

Fig. 2.4 Immersed body mesh

3 CFD Simulation flow around the flap

3.1 Mathematical model of fluid flow

The mathematical background of fluid flow is discussed in several books, which deal with fluid mechanics and numerical simulation of fluid flow.

At first, it investigated the influence of coupling the CFD with the moving body previously discussed. The effect of turbulence was modelled using standard k-ε approaches. The classical approach to modelling turbulent flows is based on averages of the Navier-Stokes equations. These are commonly called Reynolds Averaged Navier-Stokes equations (RANS). The simplest model for turbulent flow is k-ε. Even though it certainly is the best compromise for engineering design using the RANS approach.

For non-constant density flows, the Navier-Stokes equations are written in the conservative form:

Momentum equations (3.1)

$$\frac{\partial(\rho \cdot v_i)}{\partial t} + \frac{\partial(\rho \cdot v_i \cdot v_j)}{\partial x_j} =$$

$$= -\frac{\partial p}{\partial x_i} + \frac{\partial}{\partial x_j} \cdot \tau_{ij} + \rho \cdot \delta_{i3} \cdot g + \rho \cdot f_c \cdot \varepsilon_{ij3} \cdot v_j$$

$$\tau_{ij} = \mu \cdot \left(2 \cdot S_{ij} - \frac{2}{3}\delta_{ij}\frac{\partial v_i}{\partial x_j}\right);\ S_{ij} = \frac{1}{2}\left(\frac{\partial v_i}{\partial x_j} + \frac{\partial v_j}{\partial x_i}\right)$$

Continuity equation

$$\frac{\partial \rho}{\partial t} + \frac{\partial(\rho \cdot v_j)}{\partial x_j} = 0 \qquad (3.2)$$

where v is the velocity (u, v, w), t is time, x is coordinate (x, y, z), p is static pressure, ρ is density, μ is dynamic viscosity, τ_{ij} is the viscous stress tensor, S_{ij} is the rate of the strain tensor, g is gravity acceleration, δ_{i3} is Kronecker symbol ($\delta_{ij} = 1$ for $i = j$, $\delta_{ij} = 0$ for $i \neq j$), ε_{ijk} is a unit tensor ($\varepsilon_{ijk} = 1$ for $ijk = 123{,}231{,}312$, $\varepsilon_{ijk} = -1$ for $ijk = 321{,}213{,}132$, $\varepsilon_{ijk} = 0$ for other combination of ijk).

In equation (3.1), the two left terms on the left-hand side represent the local rate of change and convection of the momentum, respectively. The first term on the right side is the pressure gradient, and the second term represents molecular transport due to viscosity. The third term represents the buoyant effect, and the fourth term represents the Coriolis effect. Using Reynolds averaging on equations (3.1) and (3.2), one obtains averaged equations.

Averaged momentum equations

$$\frac{\partial(\rho \cdot \overline{v_\iota})}{\partial t} + \frac{\partial(\rho \cdot \overline{v_\iota} \cdot \overline{v_\jmath})}{\partial x_j} + \frac{\partial(\rho \cdot \overline{v_\iota{}' \cdot v_\jmath{}'})}{\partial x_j} =$$

$$= -\frac{\partial \overline{p}}{\partial x_i} + \frac{\partial}{\partial x_j} \cdot \overline{\tau_{\iota\jmath}} + \rho \cdot \delta_{i3} \cdot g + \rho \cdot f_c \cdot \varepsilon_{ij3} \cdot \overline{v_\jmath} \qquad (3.3)$$

$$\overline{\tau_{\iota\jmath}} = \mu \cdot \left(2 \cdot \overline{S_{\iota\jmath}} - \frac{2}{3} \cdot \delta_{ij} \cdot \frac{\partial \overline{v_\iota}}{\partial x_j}\right);\ \overline{S_{\iota\jmath}} = \frac{1}{2} \cdot \left(\frac{\partial \overline{v_\iota}}{\partial x_j} + \frac{\partial \overline{v_\jmath}}{\partial x_i}\right)$$

Continuity equation

$$\frac{\partial \rho}{\partial t} + \frac{\partial(\rho \cdot \overline{v_\jmath})}{\partial x_j} = 0 \qquad (3.4)$$

Equation (3.3) is like (3.1) except for the third term of the right side of the equation. The new term $\left(\rho \cdot \overline{v_\iota{}' \cdot v_\jmath{}'}\right)$ is called Reynolds stress tensor. This tensor is unknown and represents the first closure problem for turbulence modelling. It is possible to derive the equation for the six components of the Reynolds stress tensor. Although the Reynolds stress model contains a complete description of the physics, it is not yet widely used in

turbulent combustion. Many industrial codes still rely on the k−ε model, which introduces the assumption of isotropy by using an eddy viscosity. It is known that turbulence becomes isotropic at the small scales, but this does not necessarily apply to the large scale at which the averaged quantities are defined. The k−ε model is based on equations where the turbulent transport is diffusive and therefore is more easily handled by numerical method than the Reynolds stress equation. This is probably the most important reason for its wide use in many codes. An important simplification is obtained by introducing the eddy viscosity μ_t, which lead to the following expression for the Reynolds stress tensor.

$$-\rho \cdot \overline{v_i} \cdot \overline{v_j} = \mu_t \cdot \left(2 \cdot \overline{S_{ij}} - \frac{2}{3} \cdot \delta_{ij} \cdot \frac{\partial \overline{v_i}}{\partial x_j}\right) - \frac{2}{3}\delta_{ij} \cdot \rho \cdot k \qquad (3.5)$$

Where k is turbulent kinetic energy.

Turbulent kinetic energy and eddy dissipation are related to turbulent viscosity by equation.

$$\mu_t = \rho \cdot C_\mu \cdot \frac{k^2}{\varepsilon} \qquad (3.6)$$

Where ε is eddy dissipation and C_μ is constant.

The introduction of variables k, ε requires that modelled equations are available for these quantities.

Turbulent kinetic energy

$$\frac{\partial(\rho \cdot k)}{\partial t} + \frac{\partial\left(\rho \cdot \overline{v_j} \cdot k\right)}{\partial x_j} = \\ = \frac{\partial}{\partial x_j} \cdot \left(\left(\mu + \frac{\mu_t}{\sigma_k}\right) \cdot \frac{\partial k}{\partial x_j}\right) + G_k - G_b - \rho \cdot \varepsilon - Y_M \qquad (3.7)$$

Turbulent eddy dissipation

$$\frac{\partial(\rho \cdot \varepsilon)}{\partial t} + \frac{\partial\left(\rho \cdot \overline{v_j} \cdot \varepsilon\right)}{\partial x_j} = \\ = \frac{\partial}{\partial x_j} \cdot \left(\left(\mu + \frac{\mu_t}{\sigma_\varepsilon}\right) \cdot \frac{\partial \varepsilon}{\partial x_j}\right) + C_{\varepsilon 1} \frac{\varepsilon}{k} \cdot (G_k + C_{3\varepsilon} \cdot G_b) - C_{2\varepsilon} \cdot \rho \cdot \frac{\varepsilon^2}{k} \qquad (3.8)$$

Where G_k is the production of turbulent kinetic energy, G_b is the generation of turbulence due to buoyancy, and Y_M is the production of turbulence due to compressibility.

$$G_k = \mu_t \cdot \left(\frac{\partial \overline{v_j}}{\partial x_l} + \frac{\partial \overline{v_l}}{\partial x_j}\right) \cdot \frac{\partial \overline{v_j}}{\partial x_l} \\ G_b = -g_j \cdot \frac{\mu_t}{\rho \cdot \sigma_h} \cdot \frac{\partial \rho}{\partial x_j} \qquad (3.9)$$

$$\sigma_h = \frac{\mu_t}{\lambda_t} \cdot c_p$$

$$Y_M = 2 \cdot \rho \cdot \varepsilon \cdot \frac{k}{\gamma \cdot R \cdot T}$$

Where σ_h is Turbulent Prandtl number, λ_t is turbulent thermal conductivity, $and\ c_p$ is specified heat capacity.

In equations (3.7) and (3.8), the two teem on the left side represent local rate and convection, respectively. The first term on the right side represents turbulent transport, the second is turbulent production, and the third is turbulent dissipation.

3.2 Test geometry

As mentioned above, the first step consisted of the flow simulation in a "simplified" flap valve. The flap was designed not to limit any method of moving mesh. The flap was in the pipe, and the pipe does not contain any additional parts like a seal, gasket, flap stop, etc. Mesh was very similar for all models due to the relevant comparison of results, such as torque and velocity field surrounding flap, flow through the pipe, etc.

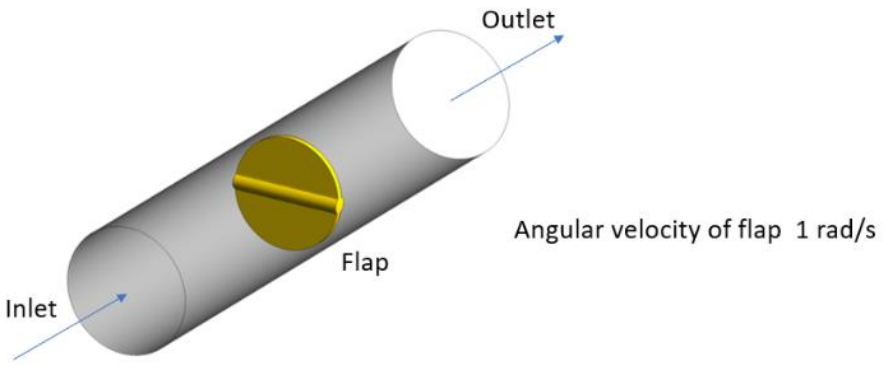

Fig. 3.1 Test geometry

The test was performed as an unsteady transient case, and the shut-off of the flap was simulated. The total pressure inlet and static pressure outlet were set as boundary conditions, which is the best combination for variable flow reaching zero.

Next, the phenomenon of moving the body in the fluid was analysed. In general, if the motion of the body is very slow relative to fluid velocity, then the transient state can be simulated as a set of stationary simulations of the flap in discrete positions (variable angle of rotation).

3.3 Test case-results

The test simulations' main goal was to compare the pressure field acting on the flap simulated by different approaches. The torque acting on the flap was monitored during the flap rotation for all solved variants. We can see that the contours of static pressure are similar. More significant are differences in velocity contours, especially for immersed body

method. Elementary principles of immersed body method can cause it. Only immersed body method does not include a cavity representing the flap's real shape, and the flap's shape is reconstructed in CFD simulation by overlapping solid and fluid mesh.

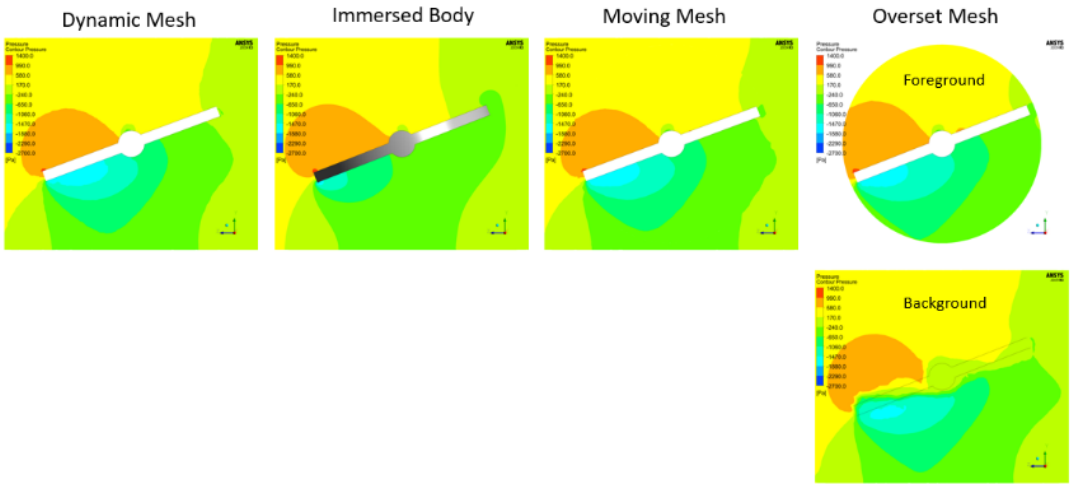

Fig. 3.2 Contours of static pressure, identical scale for all variants

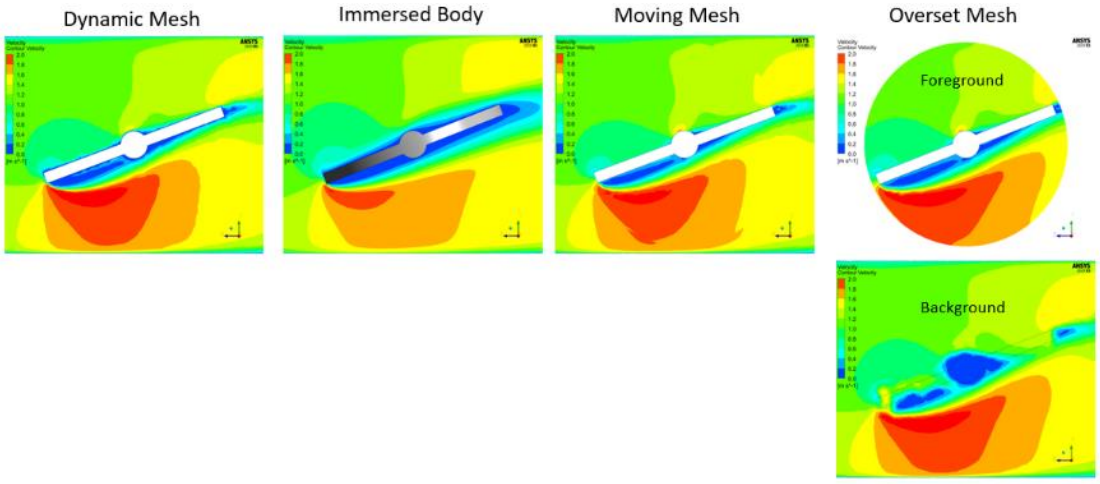

Fig. 3.3 Contours of velocity magnitude, the identical scale for all variants

The torque–time characteristics were also compared with a set of stationary solutions for the discrete angle of rotation of the flap.

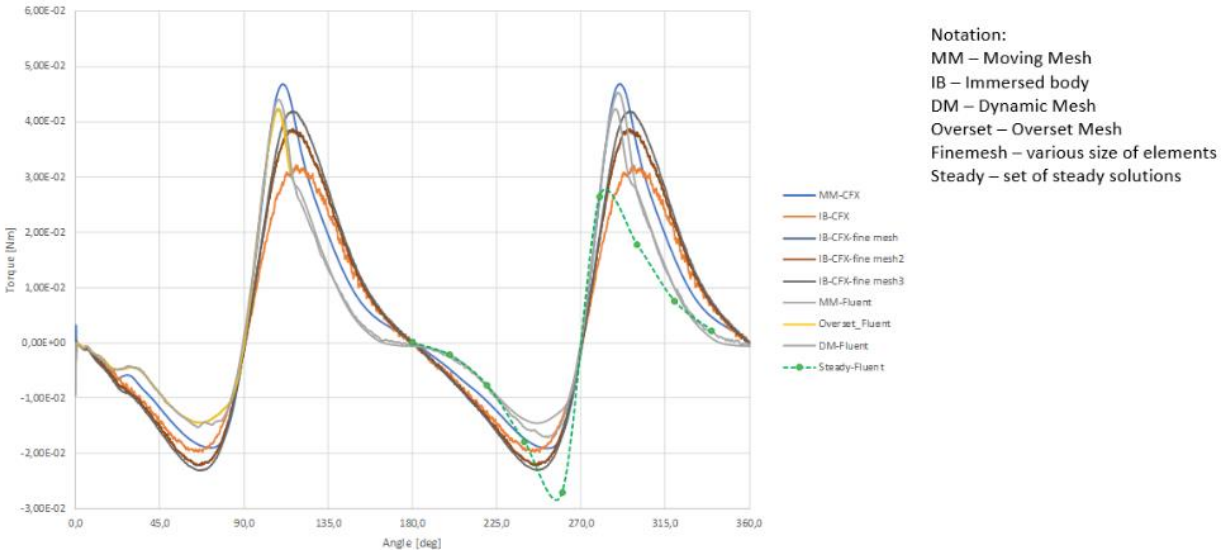

Fig. 3.4 Torque characteristics of the flap with respect to the angle of rotation

Differences between methods are evident, and the shape of the curve calculated by immersed body method is different from all other methods. As mentioned above, only immersed body method does not include the real shape of the flap in the fluid mesh. We can see that the method is very sensitive to the element size of the fluid mesh.

Flow characteristics of the flap were estimated as well. Differences are not so significant, but the immersed body method is still different from others.

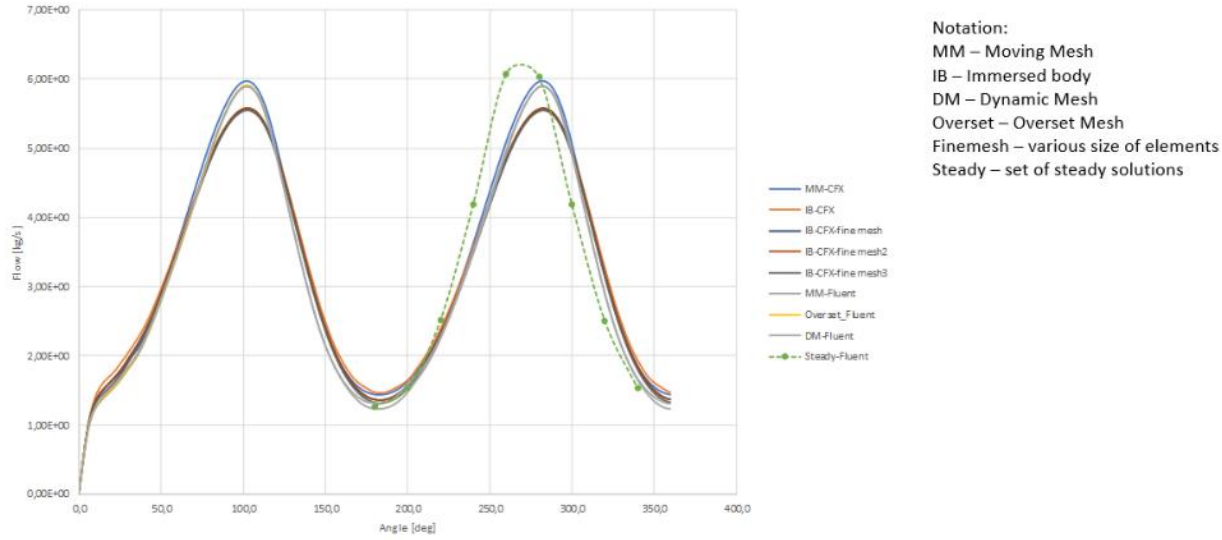

Fig. 3.5 Flow characteristics of the flap with respect to the angle of rotation

Finally, the effect of the closing speed was analysed, and the influence of the angular velocity of the flap respectively. The rotation of the flap was simulated by the moving mesh method for four angular velocities, namely 0.1, 0.2, 0.5 and 1 rad/s. The next steady state of the flap was simulated in the range of 0 - 360 degrees with step 20 degrees. These simulations represented a set of steady-state simulations and discrete points in flow-angle and torque-angle characteristics.

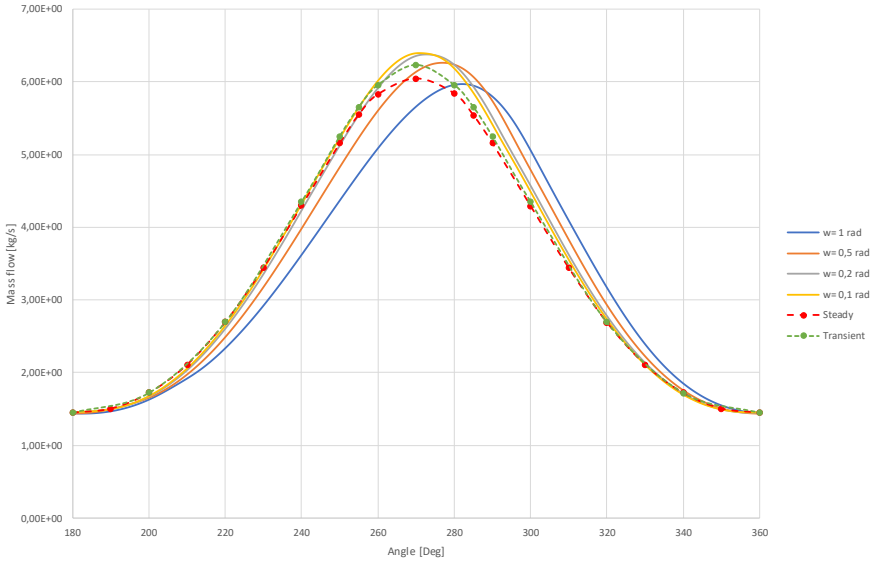

Fig. 3.6 Flow–angle characteristics for steady state set and various angular velocity transient simulation

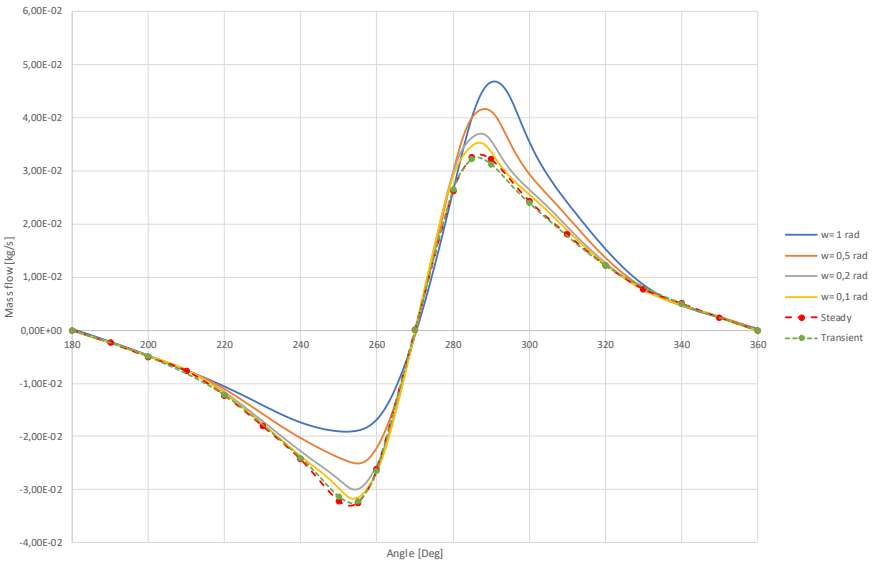

Fig. 3.7 Torque–angle characteristics for steady–state set and various angular velocity transient simulation

If the angular velocity reached zero value (limit variant), the solution would be the same. Generally speaking, if the closing or opening of the flap is slow, then the process can be simulated as a set of discrete positions of the flap (steady state). The problem is how to find out the limit angular velocity.

This project has received funding from the European High-Performance Computing Joint Undertaking (JU) under grant agreement No 951732. The JU receives support from the European Union's Horizon 2020 research and innovation programme and Germany, Bulgaria, Austria, Croatia, Cyprus, the Czech Republic, Denmark, Estonia, Finland, Greece, Hungary, Ireland, Italy, Lithuania, Latvia, Poland, Portugal, Romania, Slovenia, Spain, Sweden, the United Kingdom, France, the Netherlands, Belgium, Luxembourg, Slovakia, Norway, Switzerland, Turkey, the Republic of North Macedonia, Iceland, and Montenegro. This project has received funding from the Ministry of Education, Youth and Sports of the Czech Republic (ID:MC2101).